

Bayesian surface regression versus spatial spectral nonparametric curve regression

M.D. Ruiz–Medina and D. Miranda
IMAG - Unidad de excelencia María de Maeztu - CEX2020-001105-M

Abstract

COVID–19 incidence is analyzed at the provinces of some Spanish Communities during the period February–October, 2020. Two infinite–dimensional regression approaches are tested. The first one is implemented in the regression framework introduced in Ruiz–Medina, Miranda and Espejo [70]. Specifically, a bayesian framework is adopted in the estimation of the pure point spectrum of the temporal autocorrelation operator, characterizing the second–order structure of a surface sequence. The second approach is formulated in the context of spatial curve regression. A non–parametric estimator of the spectral density operator, based on the spatial periodogram operator, is computed to approximate the spatial correlation between curves. Dimension reduction is achieved by projection onto the empirical eigenvectors of the long–run spatial covariance operator. Cross–validation procedures are implemented to test the performance of the two functional regression approaches.

Keywords. Bayesian estimation; nonparametric estimation; spatial curve regression; spatial periodogram operator; spatial spectral density operator; surface regression.

1 Introduction

The functional linear model has been extensively studied in the Functional Data Analysis (FDA) literature (see, e.g., Hörmann and Kokoszka [32]; Horváth and Kokoszka [36]; Ramsay and Silverman [65]). Several approaches contribute to the functional linear and least–squares regression context, involving scalar/functional response, and functional regressors. Just to mention a few, we refer to smoothing spline regression, functional principal component regression, or functional partial least–squares regression (see, e.g., Cai and Hall [8]; Crambes, Kneip and Sarda [11]; Cuevas [13]; Cuevas, Febrero and Fraiman [12]; Febrero–Bande, Galeano and Gonzalez–Manteiga [20]; Marx and Eilers [52]; Ruiz–Medina [68], among others). Morris [60] presents an extensive review on functional regression, focusing on the most common techniques supported by regularization methods. Wang, Chiou and Müller [74] describe the usual

FDA methodologies, including mean and covariance analysis, dimension reduction techniques, like Functional Principal Component Analysis, and recent advances in clustering/classification, nonlinear regression, and warping techniques for functional data. Finally, we refer to the contribution by Jadhav, Koul and Lu [40], in the multivariate functional regression context, where the effect of functional covariates on the response variable is analyzed.

One can not forget the flexible semiparametric and nonparametric functional regression approaches (see, e.g., Ferraty and Vieu [24]). A semi-functional partial linear approach for regression, based on nonparametric time series, is considered in Aneiros-Pérez and Vieu [2]; [3]. Particularly, kernel functional regression has been widely applied, including the case where both, the response and the regressors are functions (see, e.g., Ferraty, Keilegom and Vieu [23], and Ferraty and Vieu [25]). In the nonparametric framework, in the case of scalar response and functional regressors, Ferraty, Goia, Salinelli and Vieu [22] present a novel approach, where the choice of the optimal direction, based on the quadratic loss function, for projection of the regressors, and the link function is achieved. A more flexible framework to model possible structural changes is contemplated in Goia and Vieu [27], reflecting the different interaction patterns between the functional regressor and response depending on the time interval considered. The benefits of sharing high-dimensional and functional data analysis techniques are reflected in the special issue edited by Goia and Vieu [28] (see also Gao, Shang and Yang [26]).

The state-space linear framework has covered a wide range of contributions in the literature on functional time series (see Bosq [7]). Indeed, since the pioneering works by Cardot [10]; Labbas and Mourid [47]; Marion and Pumo [51] and Mas [53], one can find different regularized time series predictors, accompanied by the corresponding asymptotic analysis. Several extensions, like conditional formulations (CARH(1) models), double stochastic versions, Banach-valued versions, and sparse-data based applications, have been addressed in a vast literature (see Aue, Horváth and Pellatt [5]; Aue and Klepsch [6]; Cugliari [14]; Damon and Guillas [15]; [16]; Didericksen and Kokoszka [17]; El Hajj [18]; Ferraty, Van Keilegom and Vieu [23]; Guillas [30]; [31]; Hörmann, Horváth and Reeder [34]; Horváth, Husková and Kokoszka [38]; Horváth, Kokoszka and Rice [39]; Kara-Terki and Mourid [41]; Kargin and Onatski [42]; Klepsch, Klüppelberg and Wei [43]; Kokoszka and Reimherr [44]; [45]; Kowal, Matteson and Ruppert [46]; Laukaitis [50]; Liu, Xiao and Chen [49]; Mas [54]; [55]; [56]; [57]; Mas and Menneteau [58], and Mas and Pumo [59]).

A more general treatment, beyond structural assumptions, can be found in the book by Hormann and Kokoszka [33] (see also Aue, Norinho and Hörmann [4]; Górecki, Hörmann, Horváth and Kokoszka [29]; Hörmann, Kokoszka and Nisol [35]; Horváth, Husková and Rice [37]; Kokoszka and Reimherr [44]). The nonparametric functional time series framework offers interesting alternatives (see, e.g., Aneiros-Pérez, Cao and Vilar-Fernández [1]; Ezzahrioui and Ould-Saïd [19]; Ferraty, Goia and Vieu [21]). Finally, we mention the recent contri-

butions by Li, Robinson and Shang [48], and Ruiz–Medina [69] on long–range dependence functional time series analysis, beyond the most extensive analyzed weak–dependent time series scenario.

Canale and Ruggiero [9], Petris [63] and Torres *et al.* [73] adopt a bayesian framework in the functional time series context. The present paper also considers a bayesian approach in the estimation of the eigenvalues of the auto–correlation operator, characterizing the dependence structure of the error term, in the surface regression model formulated in equation (1) below (see Ruiz–Medina, Miranda and Espejo [70]). The generalized least–squares estimator of the infinite–dimensional regression parameter vector is then computed from the resulting bayesian estimator of the inverse of the covariance matrix operator of the error term, obeying an autoregressive hilbertian time series model.

Functional spectral analysis is one of the main open research areas in the current literature on functional time series. In Panaretos and Tavakoli [61], under a weak–dependent scenario, a nonparametric estimator of the spectral density operator based on the periodogram operator is derived. The asymptotic normality of the functional discrete Fourier transform of the curve data is previously proved, under suitable functional cumulant mixing conditions, and the summability in time of the trace norm of the elements of the covariance operator family (see also Tavakoli [71]). In Panaretos and Tavakoli [62], a Karhunen–Loève–like decomposition in the temporal functional spectral domain is derived, the so–called Cramér–Karhunen–Loève representation, providing a harmonic principal component analysis of functional time series (see also some recent applications in the context of functional regression in Pham and Panaretos [64], and Rubin and Panaretos [66]). In addition, Rubin and Panaretos [67] propose simulation techniques based on the Cramér–Karhunen–Loève representation. Differences in time series dynamics are detected by hypothesis testing in the functional spectral domain in Tavakoli and Panaretos [72]. Our paper considers a spatial formulation of the nonparametric estimator of the spectral density operator derived in Panaretos and Tavakoli [61]. From this estimator, the functional entries (kernels) of the inverse of the spatial covariance matrix operator of the curve regression error are approximated. The resulting plug–in generalized least–squares estimator of the curve regression parameter vector is computed in the spatial functional spectral domain.

The two regression approaches presented are tested in a real–data example, where COVID–19 incidence is analyzed, since February until October, at the provinces of the Spanish Communities: Andalucía, Aragón, Asturias, Cantabria, Castilla La Mancha, Castilla–León, Cataluña, Comunidad de Madrid, Comunidad Valenciana, Extremadura, Galicia, la Rioja, Murcia, Navarra, País Vasco, and Canarias. Note that, after implementing hypothesis testing (see Bosq [7]; Horváth, Husková and Rice [37]), the last community is removed in the spatial curve regression analysis. The performance of both, surface and curve regressions, is tested by cross–validation. The conclusions of our empirical study are drawn in Section 5. Particularly, the observed outperformance of the spatial

curve regression approach versus the temporal surface regression could be partially supported by the spatial weak-dependent scenario displayed by our curve data set, and the high dimensionality inherent to the parameter space in the bayesian functional time series framework. Furthermore, the dimension reduction technique implemented, based on projection onto the eigenvectors of the empirical long-run spatial covariance operator, favors the computational speed. Note also that the generalized least-squares estimator of the curve regression parameter vector is computed in the spatial spectral domain, replacing convolutions by products of the corresponding spatial functional Fourier transforms. In the supplementary material, data visualization, and some additional outputs of the estimation algorithms analyzed are displayed as well.

2 Bayesian dynamical surface regression

In the following, the random variables introduced below are defined on the basic probability space (Ω, \mathcal{A}, P) , and take their values in the real separable Hilbert space H . We restrict our attention to the dynamical functional regression model (see Ruiz-Medina, Miranda and Espejo [70]):

$$Y_n = \mu + X_n^1(\beta_1) + \dots + X_n^p(\beta_p) + \varepsilon_n, \quad n \in \mathbb{Z}, \quad (1)$$

where $\mu \in H$ is the intercept, and $\beta = (\beta_1(\cdot), \dots, \beta_p(\cdot))^T \in H^p$ is the functional regression parameter vector. The operators $X_n^i \in \mathcal{S}(H)$, $i = 1, \dots, p$, are the functional regressors defining the design matrix at each time $n \in \mathbb{Z}$. Here, $\mathcal{S}(H)$ denotes the space of Hilbert-Schmidt operators on H . The response Y_n and the regression error ε_n lie on H , for each $n \in \mathbb{Z}$.

In this paper, model (1) is interpreted as a dynamical model for disease mapping, where the functional value of the response $Y_n(\cdot)$ provides the incidence or mortality log-risk map over a spatial domain \mathcal{D} at time n , $n \in \mathbb{Z}$. It is defined from a linear combination of the kernel regressors, $X_n^i = E[(Y_{n-i} - \mu) \otimes (Y_{n-i-1} - \mu)]$, $i = 1, \dots, p$, with the functional weights β_i , $i = 1, \dots, p$, to be estimated, satisfying the equation

$$\beta_i(\mathbf{z}) = w_i \mathcal{R}_i^{-1}(Y_{n-i-1})(\mathbf{z}), \quad \mathbf{z} \in \mathcal{D}, \quad \mathcal{R}_i = E[(Y_{n-i-1} - \mu) \otimes (Y_{n-i-1} - \mu)],$$

for $i = 1, \dots, p$, and for certain unknown vector $(w_1, \dots, w_p) \in \mathbb{R}^p$. Note that, as usual, \otimes denotes the tensorial product of functions. It is well-known that for $h, g \in H$, $h \otimes g \in \mathcal{S}(H)$.

As given in Ruiz-Medina, Miranda and Espejo [70], for a fixed orthonormal basis $\{\varphi_k\}_{k \geq 1}$ of H ,

$$X_n^i(\varphi_k)(\varphi_l) = \langle X_n^i(\varphi_k), \varphi_l \rangle_H = x_{k,l}^i(n), \quad k, l \geq 1, \quad \forall n \in \mathbb{Z}, \quad i = 1, \dots, p. \quad (2)$$

Indeed, since $X_n^i \in \mathcal{S}(H)$, then, $\sum_{k,l} [x_{k,l}^i(n)]^2 < \infty$, and

$$X_n^i(f) \stackrel{H}{=} \sum_{k,l} x_{k,l}^i(n) \langle f, \varphi_l \rangle_H \varphi_k, \quad \forall f \in H, \quad (3)$$

for every $n \in \mathbb{Z}$, $i = 1, \dots, p$, where $\stackrel{H}{=}$ means the equality in the norm of H .

We work under the assumption

$$E[\varepsilon_n | X_n^1, \dots, X_n^p] = 0, \quad \forall n \in \mathbb{Z}, \quad (4)$$

on the error term $\varepsilon \equiv \{\varepsilon_n, n \in \mathbb{Z}\}$, that here is interpreted as a weak-dependent H -valued process. Indeed, ε is assumed to be a zero-mean Autoregressive Hilbertian process of order one (ARH(1) process), satisfying the following state equation:

$$\varepsilon_n = \rho(\varepsilon_{n-1}) + \varepsilon_n, \quad n \in \mathbb{Z}, \quad (5)$$

where ρ denotes the autocorrelation operator, which belongs to the space of bounded linear operators $\mathcal{L}(H)$ on H , satisfying $\|\rho\|_{\mathcal{L}(H)}^k < 1$, for $k \geq k_0$, for certain $k_0 \in \mathbb{N}$. We restrict our attention to the Gaussian case, with $\{\varepsilon_n, n \in \mathbb{Z}\}$ being an H -valued Gaussian white noise in the strong sense. Equivalently, $\{\varepsilon_n, n \in \mathbb{Z}\}$ is a sequence of independent and identically distributed H -valued zero-mean Gaussian random variables with trace autocovariance operator. The underlying surface covariance structure in time of ε is then characterized in terms of the autocovariance R_0 and cross-covariance R_1 operators, given by:

$$\begin{aligned} R_0 &= E[\varepsilon_0 \otimes \varepsilon_0] = E[\varepsilon_n \otimes \varepsilon_n], \quad \forall n \in \mathbb{Z} \\ R_1 &= E[\varepsilon_0 \otimes \varepsilon_1] = E[\varepsilon_n \otimes \varepsilon_{n+1}], \quad \forall n \in \mathbb{Z}. \end{aligned}$$

Note that, under the above model assumptions (see Ruiz-Medina, Miranda and Espejo [70]):

$$\begin{aligned} \mu_{n,\mathcal{X}} &= E[Y_n | X_n^1, \dots, X_n^p] = \mu + X_n^1(\beta_1) + \dots + X_n^p(\beta_p), \quad n = 1, \dots, N \\ E[\varepsilon_i \otimes \varepsilon_j] &= \rho^{|j-i|} R_0, \quad i, j \in \mathbb{Z}, \end{aligned} \quad (6)$$

where the last identity follows from

$$\varepsilon_n = \sum_{j=0}^k \rho^j \varepsilon_{n-j} + \rho^{k+1}(\varepsilon_{n-k-1}), \quad k \geq 1,$$

obtained by applying invertibility of the ARH(1) model (see equation (3.11) in Bosq [7]).

Let us consider the functional sample Y_1, \dots, Y_N . The following matrix expression characterizes the infinite-dimensional covariance structure of the errors

(see Ruiz-Medina, Miranda and Espejo [70]):

$$\begin{aligned}
\mathbf{C} &= E \left[(\varepsilon_1, \dots, \varepsilon_N)^T \otimes (\varepsilon_1, \dots, \varepsilon_N) \right] \\
&= \begin{bmatrix} R_0 & \rho R_0 & \rho^2 R_0 & \dots & \rho^{N-1} R_0 \\ \rho R_0 & R_0 & \rho R_0 & \dots & \rho^{N-2} R_0 \\ \vdots & \dots & \dots & \dots & \vdots \\ \rho^{N-1} R_0 & \rho^{N-2} R_0 & \dots & \dots & R_0 \end{bmatrix} \\
&= \begin{bmatrix} I & \rho & \rho^2 & \dots & \rho^{N-1} \\ \rho & I & \rho & \dots & \rho^{N-2} \\ \vdots & \dots & \dots & \dots & \vdots \\ \rho^{N-1} & \rho^{N-2} & \dots & \dots & I \end{bmatrix} \\
&\times \begin{bmatrix} R_0 & 0 & 0 & \dots & 0 \\ 0 & R_0 & 0 & \dots & 0 \\ \vdots & \dots & \dots & \dots & \vdots \\ 0 & 0 & \dots & \dots & R_0 \end{bmatrix} = \boldsymbol{\rho} \mathbf{R}_0. \tag{7}
\end{aligned}$$

Under **Assumptions A1–A2** in Ruiz-Medina, Miranda and Espejo [70], Lemma 1 provides the following pure point spectral representation of the autocorrelation matrix operator $\boldsymbol{\rho}$ given in equation (7): For every $\mathbf{f} \in H^N$,

$$\boldsymbol{\rho}(\mathbf{f}) = \sum_{k \geq 1} \boldsymbol{\Psi}_k \begin{bmatrix} 1 & \lambda_k(\rho) & \dots & [\lambda_k(\rho)]^{N-1} \\ \lambda_k(\rho) & 1 & \dots & [\lambda_k(\rho)]^{N-2} \\ \vdots & \dots & \dots & \vdots \\ [\lambda_k(\rho)]^{N-1} & \dots & \dots & 1 \end{bmatrix} \boldsymbol{\Psi}_k^*(\mathbf{f}), \tag{8}$$

where for $\mathbf{g} = (g_1, \dots, g_N) \in H^N$, and $k \geq 1$,

$$\begin{aligned}
\Psi_k^*(\mathbf{g}) &= \begin{bmatrix} \psi_k & 0 & \dots & 0 \\ 0 & \psi_k & \dots & 0 \\ \vdots & \ddots & \ddots & \vdots \\ 0 & \dots & \dots & \psi_k \end{bmatrix}^* \begin{bmatrix} g_1 \\ g_2 \\ \vdots \\ g_N \end{bmatrix} \\
&= \begin{bmatrix} \langle g_1, \psi_k \rangle_H \\ \langle g_2, \psi_k \rangle_H \\ \vdots \\ \langle g_N, \psi_k \rangle_H \end{bmatrix} = \begin{bmatrix} g_{1k} \\ g_{2k} \\ \vdots \\ g_{Nk} \end{bmatrix} \\
\Psi_k \Psi_k^*(\mathbf{g}) &= \Psi_k \begin{bmatrix} g_{1k} \\ g_{2k} \\ \vdots \\ g_{Nk} \end{bmatrix} \\
&= \begin{bmatrix} \psi_k & 0 & \dots & 0 \\ 0 & \psi_k & \dots & 0 \\ \vdots & \ddots & \ddots & \vdots \\ 0 & \dots & \dots & \psi_k \end{bmatrix} \begin{bmatrix} g_{1k} \\ g_{2k} \\ \vdots \\ g_{Nk} \end{bmatrix} \\
&= \begin{bmatrix} g_{1k}\psi_k \\ g_{2k}\psi_k \\ \vdots \\ g_{Nk}\psi_k \end{bmatrix} \\
\Psi_k^* \Psi_k &= \begin{bmatrix} \langle \psi_k, \psi_k \rangle_H & 0 & \dots & 0 \\ 0 & \langle \psi_k, \psi_k \rangle_H & \dots & 0 \\ \vdots & \ddots & \ddots & \vdots \\ 0 & \dots & \dots & \langle \psi_k, \psi_k \rangle_H \end{bmatrix} \\
&= \begin{bmatrix} 1 & 0 & \dots & 0 \\ 0 & 1 & \dots & 0 \\ \vdots & \ddots & \ddots & \vdots \\ 0 & \dots & \dots & 1 \end{bmatrix}.
\end{aligned} \tag{9}$$

Here, $\{\lambda_k(\rho), k \geq 1\}$ and $\{\psi_k, k \geq 1\}$ denote the systems of eigenvalues and eigenvectors of the autocorrelation operator ρ appearing in equation (5). Lemma 3 in Ruiz-Medina, Miranda and Espejo [70] derives, under suitable conditions, the inverse of the covariance matrix operator \mathbf{C} in (7), characterizing the second-order structure of the functional regression error term. The functional entries of this inverse operator can be obtained from the eigenvalues and

eigenvectors of the autocorrelation operator ρ . Specifically, \mathbf{C}^{-1} is given by (see Lemma 3 in Ruiz-Medina, Miranda and Espejo [70]):

$$\mathbf{C}^{-1}(\mathbf{f})(\mathbf{g}) = \sum_{k,l} [\Psi_l^*(\mathbf{g})]^T \mathbf{H}_{l,k} \Psi_k^*(\mathbf{f}) \quad (10)$$

$$\mathbf{H}_{l,k} = \begin{bmatrix} a_{l,k} & b_{l,k} & 0 & \dots & 0 \\ b_{l,k} & c_{l,k} & b_{l,k} & \dots & 0 \\ \vdots & \ddots & \ddots & \ddots & \vdots \\ 0 & \dots & b_{l,k} & c_{l,k} & b_{l,k} \\ 0 & 0 & \dots & b_{l,k} & a_{l,k} \end{bmatrix}, \quad (11)$$

where $a_{l,k}, b_{l,k}, c_{l,k}$, $k, l \geq 1$, satisfy the following identities in the norm of H : For every $f \in H$,

$$\begin{aligned} \tilde{C}_{1,1}(f) &= \tilde{C}_{N,N}(f) = R_0^{-1}(I - \rho^2)^{-1}(f) \\ &= \sum_{k,l} \frac{1}{1 - \lambda_k^2(\rho)} R_0^{-1}(\psi_k)(\psi_l) \langle \psi_k, f \rangle_H \psi_l \\ &= \sum_{k,l} a_{l,k} \langle \psi_k, f \rangle_H \psi_l \\ \tilde{C}_{i,i+1}(f) &= \tilde{C}_{j,j-1}(f) = -R_0^{-1}(I - \rho^2)^{-1}\rho(f) \\ &= -\sum_{k,l} \frac{\lambda_k(\rho)}{1 - \lambda_k^2(\rho)} R_0^{-1}(\psi_k)(\psi_l) \langle \psi_k, f \rangle_H \psi_l \\ &= \sum_{k,l} b_{l,k} \langle \psi_k, f \rangle_H \psi_l, \quad i = 1, \dots, N-1, \quad j = 2, \dots, N \\ \tilde{C}_{i,i}(f) &= R_0^{-1}(I - \rho^2)^{-1}(I + \rho^2)(f) \\ &= \sum_{k,l} \frac{1 + \lambda_k^2(\rho)}{1 - \lambda_k^2(\rho)} R_0^{-1}(\psi_k)(\psi_l) \langle \psi_k, f \rangle_H \psi_l \\ &= \sum_{k,l} c_{l,k} \langle \psi_k, f \rangle_H \psi_l, \quad i = 2, \dots, N-1. \end{aligned} \quad (12)$$

2.1 Bayesian estimation

As given in equation (24) in Ruiz-Medina, Miranda and Espejo [70], the generalized least-squares estimator $\hat{\beta}_N$ of the parameter vector $\beta \in H^p$, can be computed from equations (11)–(12) as follows:

$$\begin{aligned} \hat{\beta}_N &:= \min_{\beta \in H^p} L^2(\beta) = \min_{\beta \in H^p} \|\mathbf{Y} - \mathbf{X}(\beta)\|_{\mathcal{H}(\epsilon)}^2 \\ &= \min_{\beta \in H^p} (\mathbf{Y} - \mathbf{X}(\beta))^T \mathbf{C}^{-1}(\mathbf{Y} - \mathbf{X}(\beta)) \\ &= \min_{\beta \in H^p} \sum_{k,l} [\Psi_l^*(\mathbf{Y} - \mathbf{X}(\beta))]^T \mathbf{H}_{l,k} \Psi_k^*(\mathbf{Y} - \mathbf{X}(\beta)). \end{aligned} \quad (13)$$

We propose here a Bayesian estimation of $\cdot\lambda_k(\rho)$ in equation (12), for every $k \geq 1$. Hence, the entries of matrixes $\mathbf{H}_{l,k}$, $k, l \geq 1$, are approximated from equation (12) by replacing R_0 by its empirical version, given by $\widehat{R}_0^{(N)} = \frac{1}{N} \sum_{t=1}^N \varepsilon_t \otimes \varepsilon_t$, and $\lambda_k(\rho)$, $k \geq 1$, by their bayesian estimates. Indeed, a truncated version of equation (12) is considered. Specifically, we consider the truncated pure point spectral diagonal expansion

$$\widehat{R}_0^{(k(N))} = \sum_{k=1}^{k(N)} \widehat{\lambda}_{k,N} \widehat{\phi}_{k,N} \otimes \widehat{\phi}_{k,N}, \quad (14)$$

where $\widehat{R}_0^{(k(N))} \widehat{\phi}_{k,N} = \widehat{\lambda}_{k,N} \widehat{\phi}_{k,N}$, for $k = 1, \dots, k(N)$. Here, $k(N) < N$ such that $k(N)/N \rightarrow 0$, $N \rightarrow \infty$, with a certain velocity decay to ensure strong-consistency (see Bosq [7]). Usually, $k(N) = \ln(N)$ is a suitable choice. For $k = 1, \dots, k(N)$, the bayesian estimator $\widehat{\lambda}_k(\rho)$ of $\lambda_k(\rho)$ is computed by maximizing the posterior probability density. Namely, for

$$\Delta_\rho(\varepsilon) = \{\varepsilon_2(\psi_k) - \lambda_k(\rho)\varepsilon_1(\psi_k), \dots, \varepsilon_N(\psi_k) - \lambda_k(\rho)\varepsilon_{N-1}(\psi_k)\}_{k=1, \dots, k(N)},$$

with $\varepsilon = (\varepsilon_1, \dots, \varepsilon_N)$, and for $\boldsymbol{\lambda}(\rho) = (\lambda_1(\rho), \dots, \lambda_{k(N)}(\rho))$, under the Gaussian distribution of the errors, the posterior probability density $\widetilde{L}_{k(N)}(\boldsymbol{\lambda}(\rho)/\varepsilon) = \widetilde{L}_{k(N)}(\boldsymbol{\lambda}(\rho)/\Delta_\rho(\varepsilon))$ can be written as

$$\begin{aligned} & \widetilde{L}_{k(N)}(\lambda_1(\rho), \dots, \lambda_{k(N)}(\rho)/\Delta_\rho(\varepsilon)) \\ & \simeq L_N(\Delta_\rho(\varepsilon)/\lambda_1(\rho), \dots, \lambda_{k(N)}(\rho)) p_{k(N)}(\lambda_1(\rho), \dots, \lambda_{k(N)}(\rho)) \\ & = \prod_{k=1}^{k(N)} \left[\frac{1}{\sigma_k^N (2\pi)^{N/2}} \exp\left(-\frac{1}{2\sigma_k^2} \sum_{t=1}^N [\varepsilon_t(\psi_k)]^2\right) \right. \\ & \quad \left. \times [\lambda_k(\rho)]^{a_k-1} (1 - \lambda_k(\rho))^{b_k-1} \frac{\mathbb{I}_{\{0 < \lambda_k(\rho) < 1\}}}{\mathbb{B}(a_k, b_k)} \right], \end{aligned} \quad (15)$$

where we work under the assumption that $\boldsymbol{\lambda}(\rho) = (\lambda_1(\rho), \dots, \lambda_{k(N)}(\rho))$ is a vector of $k(N)$ independent beta random variables with respective shape parameters a_k and b_k , $k = 1, \dots, k(N)$, under the joint prior probability density $p_{k(N)}$, where, as usual, $\mathbb{I}_{0 < \cdot < 1}$ denotes the indicator function on the interval $(0, 1)$, and $\mathbb{B}(a_k, b_k)$ is the beta function,

$$\mathbb{B}(a_k, b_k) = \frac{\Gamma(a_k)\Gamma(b_k)}{\Gamma(a_k + b_k)}, \quad k = 1, \dots, k(N).$$

We have also applied the independence of the components of the innovation process ε under the Gaussian strong-white noise assumption. Hence, for each $k = 1, \dots, k(N)$, $\varepsilon_t(\psi_k) = \langle \varepsilon_t, \psi_k \rangle_H$, and $\sigma_k = \sqrt{E[\varepsilon_t(\psi_k)]^2}$, for $t = 1, \dots, N$. In (15), \simeq means identity except a positive constant \mathcal{K} , since $\widetilde{L}_{k(N)}(\lambda_1(\rho), \dots, \lambda_{k(N)}(\rho)/\Delta_\rho(\varepsilon))$ is proportional to the likelihood function

$L_N(\Delta_\rho(\varepsilon)/\lambda(\rho))$ and the prior joint probability density $p_{k(N)}(\lambda(\rho))$. Thus, \mathcal{K} is given by

$$\mathcal{K} = \int_{\Lambda} L_N(\varepsilon/\lambda(\rho)) p_{k(N)}(\lambda(\rho)) d\lambda(\rho).$$

For $i, j = 1, \dots, N$, the following approximation $\widehat{C}_{i,j}$ to $\widetilde{C}_{i,j}$ in (12) is obtained, by replacing R_0 by its truncated empirical version $\widehat{R}_0^{(k(N))}$ in (14), and $\lambda_k(\rho)$ by its bayesian estimate $\widehat{\lambda}_k(\rho)$, for $k = 1, \dots, k(N)$,

$$\begin{aligned} \widehat{C}_{1,1}(f) &= \widehat{C}_{N,N}(f) = [\widehat{R}_0^{(k(N))}]^{-1} (I - \widehat{\rho}_{k(N)}^2)^{-1} (f) \\ &= \sum_{k,l=1}^{k(N)} \frac{1}{1 - \widehat{\lambda}_k^2(\rho)} [\widehat{R}_0^{(k(N))}]^{-1} (\psi_k)(\psi_l) \langle \psi_k, f \rangle_H \psi_l \\ &= \sum_{k,l=1}^{k(N)} \widehat{a}_{l,k}^{(N)} \langle \psi_k, f \rangle_H \psi_l \\ \widehat{C}_{i,i+1}(f) &= \widehat{C}_{j,j-1}(f) = -[\widehat{R}_0^{(k(N))}]^{-1} (I - \widehat{\rho}_{k(N)}^2)^{-1} \widehat{\rho}_{k(N)} (f) \\ &= - \sum_{k,l}^{k(N)} \frac{\widehat{\lambda}_k(\rho)}{1 - \widehat{\lambda}_k^2(\rho)} [\widehat{R}_0^{(k(N))}]^{-1} (\psi_k)(\psi_l) \langle \psi_k, f \rangle_H \psi_l \\ &= \sum_{k,l}^{k(N)} \widehat{b}_{l,k}^{(N)} \langle \psi_k, f \rangle_H \psi_l, \quad i = 1, \dots, N-1, \quad j = 2, \dots, N \\ \widehat{C}_{i,i}(f) &= [\widehat{R}_0^{(k(N))}]^{-1} (I - \widehat{\rho}_{k(N)}^2)^{-1} (I + \widehat{\rho}_{k(N)}^2) (f) \\ &= \sum_{k,l=1}^{k(N)} \frac{1 + \widehat{\lambda}_k^2(\rho)}{1 - \widehat{\lambda}_k^2(\rho)} [\widehat{R}_0^{(k(N))}]^{-1} (\psi_k)(\psi_l) \langle \psi_k, f \rangle_H \psi_l \\ &= \sum_{k,l}^{k(N)} \widehat{c}_{l,k}^{(N)} \langle \psi_k, f \rangle_H \psi_l, \quad i = 2, \dots, N-1, \end{aligned} \tag{16}$$

for any $f \in H$, where $\widehat{\rho}_{k(N)} = \sum_{k=1}^{k(N)} \widehat{\lambda}_k(\rho) \psi_k \otimes \psi_k$. From equations (10)–(12), and (16), the inverse \mathbf{C}^{-1} of the covariance matrix operator \mathbf{C} is approximated by $\widehat{\mathbf{C}}_{B,N}^{-1}$, given by

$$\widehat{\mathbf{C}}_{B,N}^{-1} = \sum_{k,l}^{k(N)} [\Psi_l^*(\mathbf{g})]^T \widehat{H}_{l,k}^{(N)} \Psi_k^*, \tag{17}$$

where, for $k, l = 1, \dots, k(N)$, $\widehat{H}_{l,k}^{(N)}$ has entries $\widehat{a}_{l,k}^{(N)}$, $\widehat{b}_{l,k}^{(N)}$ and $\widehat{c}_{l,k}^{(N)}$ computed from (16).

Under **Assumptions A1–A4** in Ruiz-Medina, Miranda and Espejo [70], the plug-in bayesian estimator we obtain for the functional parameter vector β is given by

$$\begin{aligned}
\widehat{\boldsymbol{\beta}}_{B,N} &= \left(\mathbf{X}^T \widehat{\mathbf{C}}_{B,N}^{-1} \mathbf{X} \right)^{-1} \mathbf{X}^T \widehat{\mathbf{C}}_{B,N}^{-1} (\mathbf{Y}_N) \\
&= \boldsymbol{\beta} + \left(\mathbf{X}^T \widehat{\mathbf{C}}_{B,N}^{-1} \mathbf{X} \right)^{-1} \mathbf{X}^T \widehat{\mathbf{C}}_{B,N}^{-1} (\boldsymbol{\varepsilon}_N).
\end{aligned} \tag{18}$$

From (18), the corresponding bayesian functional regression predictor is computed as

$$\widehat{\mathbf{Y}}_{B,N} = \mathbf{X} \widehat{\boldsymbol{\beta}}_{B,N}. \tag{19}$$

2.2 Estimation algorithm 1

We briefly summarize the main steps we have followed in the implementation of the functional regression estimation methodology above-introduced, to compute the predictor $\widehat{\mathbf{Y}}_{B,N}$, from the real-data set analyzed in Section 4.1 on COVID-19 incidence in some Spanish Communities.

- Step 1** Temporal interpolation and cubic B-spline smoothing is achieved over the COVID-19 cumulative cases step curves located at each one of the Spanish provinces analyzed. Their derivatives and logarithmic transform are then computed. Spatial interpolation is also implemented.
- Step 2** Bayesian componentwise estimation of the functional entries of the inverse \mathbf{C}^{-1} of the covariance matrix operator \mathbf{C} (see equations (16)–(17)), in terms of the truncated empirical autocovariance operator, and the bayesian estimates of the eigenvalues of the autocorrelation operator.
- Step 3** Computation of the generalized least-squares estimator $\widehat{\boldsymbol{\beta}}_{B,N} = \left(\widehat{\beta}_{B,N}^1, \dots, \widehat{\beta}_{B,N}^p \right)$ of the regression parameter vector $\boldsymbol{\beta}$ from equations (13)–(18).
- Step 4** Computation of the bayesian predictor $\widehat{\mathbf{Y}}_{B,N}$ from **Step 3**, as given in equation (19).
- Step 5** Model fitting is evaluated in terms of cross-validation.

3 Spatial functional multiple regression approach in the spectral domain

Let $X = \{X_{\mathbf{z}}, \mathbf{z} \in \mathbb{Z}^d\}$ be a spatial functional time series with values in the real separable Hilbert space $\mathcal{H} = L^2([\mathcal{T}_1, \mathcal{T}_2], \mu(dt))$, $T_i \in (-\infty, \infty)$, $i = 1, 2$. Here, $\mu(\cdot)$ is a finite positive measure, whose support is the time interval $[\mathcal{T}_1, \mathcal{T}_2]$. For every $\mathbf{z} \in \mathbb{Z}^d$, $P[X_{\mathbf{z}} \in L^2([\mathcal{T}_1, \mathcal{T}_2], \mu(dt))] = 1$, i.e., $X_{\mathbf{z}}$ is a random element in $L^2([\mathcal{T}_1, \mathcal{T}_2], \mu(dt))$.

Assume that X is stationary in space and has zero mean. The kernels $\{\tilde{r}_{\mathbf{z},\mathbf{y}}, \mathbf{z}, \mathbf{y} \in \mathbb{Z}^d\}$

$$\tilde{r}_{\mathbf{z},\mathbf{y}}(\tau, \sigma) = E[X_{\mathbf{z}}(\tau)X_{\mathbf{y}}(\sigma)] = r_{\mathbf{x}}(\tau, \sigma), \quad \tau, \sigma \in [\mathcal{T}_1, \mathcal{T}_2], \quad \mathbf{x} = \mathbf{z} - \mathbf{y} \in \mathbb{Z}^d$$

respectively define the spatial covariance operators $\{\tilde{\mathcal{R}}_{\mathbf{z},\mathbf{y}}, \mathbf{z}, \mathbf{y} \in \mathbb{Z}^d\}$. Thus, for $\mathbf{y}, \mathbf{z} \in \mathbb{Z}^d$, with $\mathbf{x} = \mathbf{z} - \mathbf{y}$,

$$\begin{aligned} \tilde{\mathcal{R}}_{\mathbf{z}-\mathbf{y}}(f)(g) &= E[X_{\mathbf{z}} \otimes X_{\mathbf{y}}](f)(g) = \mathcal{R}_{\mathbf{x}}(f)(g) \\ &= E \left[\langle X_{\mathbf{z}}, g \rangle_{L^2([\mathcal{T}_1, \mathcal{T}_2], \mu(dt))} \langle X_{\mathbf{y}}, f \rangle_{L^2([\mathcal{T}_1, \mathcal{T}_2], \mu(dt))} \right] \\ &\quad \forall f, g \in L^2([\mathcal{T}_1, \mathcal{T}_2], \mu(dt)). \end{aligned} \quad (20)$$

In particular, if in equation (20) we consider $\mathbf{z} = \mathbf{y}$ we obtain the definition of the spatial autocovariance operator \mathcal{R}_0 satisfying

$$\mathcal{R}_0 = E[X_{\mathbf{z}} \otimes X_{\mathbf{z}}] \in \mathcal{L}^1(L^2([\mathcal{T}_1, \mathcal{T}_2], \mu(dt))), \quad \forall \mathbf{z} \in \mathbb{Z}^d,$$

where $\mathcal{L}^1(L^2([\mathcal{T}_1, \mathcal{T}_2], \mu(dt)))$ denotes the space of trace operators on $L^2([\mathcal{T}_1, \mathcal{T}_2], \mu(dt))$. Equivalently,

$$\|\mathcal{R}_0\|_{\mathcal{L}^1(L^2([\mathcal{T}_1, \mathcal{T}_2], \mu(dt)))} = \sum_{k \geq 1} \lambda_k(\mathcal{R}_0) = E\|X_{\mathbf{z}}\|_{L^2([\mathcal{T}_1, \mathcal{T}_2], \mu(dt))}^2 = \sigma_X^2 < \infty,$$

with $\mathcal{R}_0\phi_k = \lambda_k(\mathcal{R}_0)\phi_k$, in $L^2([\mathcal{T}_1, \mathcal{T}_2], \mu(dt))$, for every $k \geq 1$. Here, $\{\phi_k\}_{k \geq 1}$ and $\{\lambda_k(\mathcal{R}_0)\}_{k \geq 1}$ respectively denote the orthonormal system of eigenvectors and associated system of eigenvalues of operator \mathcal{R}_0 .

The estimation methodology proposed is implemented in the spatial functional spectral domain. The spatial functional spectrum of X is defined in terms of the spectral density operator family $\{\mathcal{F}_{\boldsymbol{\omega}}, \boldsymbol{\omega} \in [-\pi, \pi]^d\}$, characterizing its spatial second-order structure. Particularly, we consider a family of spatial frequency varying integral operators, whose kernels lie in the space $L^2([\mathcal{T}_1, \mathcal{T}_2]^2, \mu \otimes \mu(dt, ds), \mathbb{C})$, and are given by, for each $\boldsymbol{\omega} \in [-\pi, \pi]^d$, and $\tau, \sigma \in [\mathcal{T}_1, \mathcal{T}_2]$,

$$f_{\boldsymbol{\omega}}(\tau, \sigma) \underset{L^2([\mathcal{T}_1, \mathcal{T}_2]^2, \mu \otimes \mu(dt, ds), \mathbb{C})}{=} \frac{1}{(2\pi)^d} \sum_{\mathbf{x} \in \mathbb{Z}^d} \exp(-i \langle \boldsymbol{\omega}, \mathbf{x} \rangle) r_{\mathbf{x}}(\tau, \sigma), \quad (21)$$

where $\underset{L^2([\mathcal{T}_1, \mathcal{T}_2]^2, \mu \otimes \mu(dt, ds), \mathbb{C})}{=}$ means the identity in the norm of the space $L^2([\mathcal{T}_1, \mathcal{T}_2]^2, \mu \otimes \mu(dt, ds), \mathbb{C})$.

For each $\boldsymbol{\omega} \in [-\pi, \pi]^d$, the nonparametric estimator of the spectral density operator $\mathcal{F}_{\boldsymbol{\omega}}$ we will compute later is based on the spatial functional Discrete Fourier Transform (SfDFT), and periodogram operator we now introduce.

Definition 1 The SfDFT of $\{X_{\mathbf{z}}(\tau), \tau \in [\mathcal{T}_1, \mathcal{T}_2], \mathbf{z} \in [1, T]^d \cap \mathbb{Z}^d\}$ is defined as

$$\tilde{X}_{\boldsymbol{\omega}}^{(\mathbf{N})}(\tau) = ((2\pi)^d \mathbf{N})^{-1/2} \sum_{\mathbf{z} \in [1, T]^d \cap \mathbb{Z}^d} X_{\mathbf{z}}(\tau) \exp(-i \langle \boldsymbol{\omega}, \mathbf{z} \rangle), \quad (22)$$

for all $\tau \in [\mathcal{T}_1, \mathcal{T}_2]$, and $\boldsymbol{\omega} \in \{2\pi \mathbf{z}/T, \mathbf{z} \in [1, T-1]^d\}$ where $\mathbf{N} = T^d$, and the series (22) converges in the $L^2([\mathcal{T}_1, \mathcal{T}_2], \mu(dt), \mathbb{C})$ norm.

The periodogram operator, denoted as $\mathcal{I}_{\boldsymbol{\omega}}^{(\mathbf{N})}$, is computed from the SfDFT as follows:

$$\begin{aligned} \mathcal{I}_{\boldsymbol{\omega}}^{(\mathbf{N})}(\tau, \zeta) &= \tilde{X}_{\boldsymbol{\omega}}^{(\mathbf{N})}(\tau) \overline{\tilde{X}_{\boldsymbol{\omega}}^{(\mathbf{N})}(\zeta)} = \frac{1}{((2\pi)^d \mathbf{N})} \\ &\times \left[\sum_{\mathbf{z} \in [1, T]^d \cap \mathbb{Z}^d} X_{\mathbf{z}}(\tau) \exp(-i \langle \boldsymbol{\omega}, \mathbf{z} \rangle) \right] \overline{\left[\sum_{\mathbf{z} \in [1, T]^d \cap \mathbb{Z}^d} X_{\mathbf{z}}(\zeta) \exp(-i \langle \boldsymbol{\omega}, \mathbf{z} \rangle) \right]} \\ &\quad \forall (\tau, \zeta) \in [\mathcal{T}_1, \mathcal{T}_2]^2, \boldsymbol{\omega} \in \left\{ 2\pi \mathbf{z}/T, \mathbf{z} \in [1, T-1]^d \right\} \end{aligned} \quad (23)$$

where convergence holds in the $L^2([\mathcal{T}_1, \mathcal{T}_2]^2, \mu \otimes \mu(dt, ds), \mathbb{C})$ norm.

We consider the following nonparametric estimator of the spatial spectral density operator kernel:

$$\begin{aligned} \hat{f}_{\boldsymbol{\omega}}^{(\mathbf{N})}(\tau, \zeta) &= \left[\frac{(2\pi)^d}{\mathbf{N}} \right] \sum_{\mathbf{z} \in [1, T-1]^d} W^{(\mathbf{N})} \left(\boldsymbol{\omega} - \frac{2\pi \mathbf{z}}{T} \right) \mathcal{I}_{2\pi \mathbf{z}/T}^{(\mathbf{N})}(\tau, \zeta) \\ &\quad \forall (\tau, \zeta) \in [\mathcal{T}_1, \mathcal{T}_2]^2, \end{aligned} \quad (24)$$

where the weight function $W^{(\mathbf{N})}$ is given by

$$W^{(\mathbf{N})}(\mathbf{z}) = \sum_{\mathbf{j} \in \mathbb{Z}^d} \frac{1}{B_{\mathbf{N}}} W \left(\frac{\mathbf{z} + 2\pi \mathbf{j}}{B_{\mathbf{N}}} \right), \quad \mathbf{z} \in \mathbb{R}^d, \quad (25)$$

with $B_{\mathbf{N}}$ being the positive bandwidth parameter, and W satisfying

- (1) W is positive, even, and bounded in variation
- (2) $W(\mathbf{x}) = 0$, if $\|\mathbf{x}\| \geq 1$;
- (3) $\int_{\mathbb{R}^d} |W(\mathbf{x})|^2 d\mathbf{x} < \infty$
- (4) $\int_{\mathbb{R}^d} W(\mathbf{x}) d\mathbf{x} = 1$.

Particularly, after computing the nonparametric estimator (24) of the spectral density operator, the functional entries of the spatial covariance matrix operator

\mathbf{C} of the curve observations

$$\mathbf{C} = \left\{ \begin{bmatrix} r_{\mathbf{0}}(\tau, \sigma) & \dots & r_{\mathbf{0}, \dots, T-1}(\tau, \sigma) \\ \vdots & \vdots & \vdots \\ r_{T-1, \dots, \mathbf{0}}(\tau, \sigma) & \dots & r_{T-1, \dots, T-1}(\tau, \sigma) \end{bmatrix}, (\tau, \sigma) \in [\mathcal{T}_1, \mathcal{T}_2]^2 \right\}$$

are approximated, by applying the inverse SfDFT, obtaining

$$\widehat{r}_{\mathbf{x}}(\tau, \sigma) \stackrel{L^2([\mathcal{T}_1, \mathcal{T}_2]^2, \mu \otimes \mu(dt, ds))}{=} \sum_{\boldsymbol{\omega}} \widehat{f}_{\boldsymbol{\omega}}^{(\mathbf{N})}(\tau, \sigma) \exp(i \langle \boldsymbol{\omega}, \mathbf{x} \rangle), \quad (26)$$

for all $\tau, \sigma \in [\mathcal{T}_1, \mathcal{T}_2]$, and for each $\mathbf{x} \in [0, T-1]^d$. Thus, we obtain the estimator $\widehat{\mathbf{C}}_{S, \mathbf{N}}$ of \mathbf{C} , given by

$$\widehat{\mathbf{C}}_{S, \mathbf{N}} \left\{ \begin{bmatrix} \widehat{r}_{\mathbf{0}}(\tau, \sigma) & \dots & \widehat{r}_{\mathbf{0}, \dots, T-1}(\tau, \sigma) \\ \vdots & \vdots & \vdots \\ \widehat{r}_{T-1, \dots, \mathbf{0}}(\tau, \sigma) & \dots & \widehat{r}_{T-1, \dots, T-1}(\tau, \sigma) \end{bmatrix}, (\tau, \sigma) \in [\mathcal{T}_1, \mathcal{T}_2]^2 \right\}. \quad (27)$$

The plug-in generalized least-squares estimator $\widehat{\boldsymbol{\beta}}_{S, \mathbf{N}}$ of $\boldsymbol{\beta}$, and the corresponding functional regression predictor $\widehat{\mathbf{Y}}_{S, \mathbf{N}}$ are then obtained from the following identities:

$$\begin{aligned} \widehat{\boldsymbol{\beta}}_{S, \mathbf{N}} &= \left(\mathbf{X}^T \widehat{\mathbf{C}}_{S, \mathbf{N}}^{-1} \mathbf{X} \right)^{-1} \mathbf{X}^T \widehat{\mathbf{C}}_{S, \mathbf{N}}^{-1} (\mathbf{Y}_N) \\ \widehat{\mathbf{Y}}_{S, \mathbf{N}} &= \mathbf{X} \widehat{\boldsymbol{\beta}}_{S, \mathbf{N}} \\ &= \mathbf{X} \left(\left(\mathbf{X}^T \widehat{\mathbf{C}}_{S, \mathbf{N}}^{-1} \mathbf{X} \right)^{-1} \mathbf{X}^T \widehat{\mathbf{C}}_{S, \mathbf{N}}^{-1} (\mathbf{Y}_N) \right). \end{aligned} \quad (28)$$

Here, \mathbf{X} is defined from the spatial formulation of equation (1), leading to the definition of the kernel regressors $X_{\mathbf{z}}^{ij} = E[(Y_{\mathbf{z}-\mathbf{h}_i} - \boldsymbol{\mu}) \otimes (Y_{\mathbf{z}-\mathbf{h}_j} - \boldsymbol{\mu})]$, with $\mathbf{h}_i, \mathbf{h}_j, i, j = 1, \dots, p$, being the non-negative vectors of spatial lags, involved in the definition of the nearest neighborhood of the curve response value at \mathbf{z} , keeping in mind its significative spatial interactions with other spatial functional values.

3.1 Estimation algorithm 2

We now formulate the main steps of the estimation algorithm implemented, to compute the spatial functional spectral predictor $\widehat{\mathbf{Y}}_{S, \mathbf{N}}$, in the statistical analysis of the COVID-19 incidence, from the reported cases during the period February—October, 2020, at some Spanish Communities.

- Step 1** After temporal interpolation and cubic B-spline smoothing of the cumulative cases step curves located at each one of the Spanish provinces analyzed, their derivatives and logarithmic transform are computed. Again, spatial interpolation to a 10×10 regular grid is performed.
- Step 2** Tapering the spatiotemporal data, and compute the empirical long-run spatial covariance operator.
- Step 3** Compute the singular value decomposition of the empirical long-run spatial covariance operator obtained in **Step 2**.
- Step 4** Apply the SfDFT to the tapered spatial log-intensity curves, after their projection onto the selected empirical right eigenvectors of the long-run spatial covariance operator. Namely, the choice $M = 5$ for the truncation parameter is made, explaining a 99% of the empirical variability.
- Step 5** Computation of the projected spatial periodogram operator is then achieved.
- Step 6** The nonparametric estimator of the spatial spectral density operator is calculated by defining W from the modified Bartlett–Hann window.
- Step 7** Equation (28) is implemented in the projected spatial functional spectral domain.
- Step 8** The inverse SfDFT applied to the output of **Step 7** then leads to the spatial curve regression predictor $\hat{Y}_{S,N}$ in equation (28).
- Step 9** The curves at the nodes of the first row and column of the initial 10×10 regular grid are considered in the definition of the random initial condition to run 9-fold cross validation. At the n th iteration of this procedure ($n = 1, \dots, 9$), the curves located at the nodes in the n th row and n th column of the 9×9 grid define the target spatial curve sample. The remaining curves conform the training spatial functional sample.

4 Spanish COVID–19 incidence analysis

Data are obtained from the declaration of COVID–19 cases by the National Epidemiological Surveillance Network (RENAVE), through the computer platform via the Web SiViES (Spanish Surveillance System), managed by the National Epidemiology Center (CNE). This information comes from the epidemiological case survey that each Autonomous Community completes upon the identification of COVID-19 cases. The provinces and Autonomous Communities are indicated by the ISO 3166-2 code published by the International Standardization Organization (ISO). An acceptable quality of the records drives the selection procedure of the Spanish Communities analyzed during the period February–October, 2020.

4.1 Estimation algorithm one

A functional sample of size $N = 1061$ of COVID–19 incidence log–risk surfaces, covering the area of the Spanish Communities analyzed, is obtained after applying functional data (FD) preprocessing (see **Step 1** in Section 2.2). Edge effects are removed by reducing to 1000 the number of temporal nodes defining the surface sample size. We find here an important difference regarding implementation of estimation algorithm 2 where data tapering is applied.

After removing the intercept μ , least–squares 2–D polynomial fitting is implemented to approximate kernel regressors in model (1) from their empirical version, applying 'fit' MatLab function. Our polynomial choice in the argument of *fit* function corresponds to the best goodness of fit reported in *gof* output of *fit* function. To implement **Step 2**, based on bayesian estimation of the residual correlation structure, ordinary least squares is first applied in terms of the computed functional design matrix, following similar steps to the ones described in Section 4 in [70], under the choice $k(N) = \ln(N)$ of the truncation parameter. Note that conditions of Proposition 1 in [70] hold under the kernel polynomial fitting previously achieved. The beta shape hyperparameters $a_k, b_k, k = 1, \dots, k(N)$, for the prior in equation (15), are selected according to the bootstrap probability density fitted to the eigenvalues of the empirical correlation structure of the ordinary least–squares residuals (see Step 8 of the estimation algorithm proposed in Torres *et al.* [73] for the statistical analysis of COVID–19 mortality). To compute equation (16), equation (15) is maximized following a similar procedure to Step 9 in Torres *et al.* [73], from *gaoptimset* MaLab function (selecting *HybridFcn* option). The selected option of *gaoptimset* function runs a hybrid genetic algorithm, involving quasi–Newton methodology in the optimization procedure applied after the genetic algorithm finishes. The corresponding outputs allows us to implement **Step 3**, where a bayesian approximation (18) to equation (13), in terms of $\widehat{\mathbf{C}}_{B,N}^{-1}$, is obtained from equations (16)–(17) computed in **Step 2**. **Step 4** follows straightforward from **Steps 1–3**, and equation (19).

Finally, Leave–One Out Cross Validation (LOOCV) is implemented from **Step 1–4**. Specifically, our training sample is obtained by removing one surface at each iteration of the cross–validation procedure. This surface is considered as the target output to be compared with the output of the corresponding iteration after implementing **Steps 1–4**. Note that the reduced sample after eliminating edge effects, and removing the initial times, where the random initial conditions are defined, has size 993. The ℓ^1 –norm of the computed functional error at each one of the iterations is also calculated. Its mean value over the 993 iterations is reflected in Table 1, when we restrict our attention to ten of the sixteen communities initially analyzed: Andalucía (AN) (Almería (AL), Cádiz (CA), Córdoba (CO), Granada (GR), Huelva (H), Jaén (J), Málaga (MA), Sevilla (SE)); Aragón (AR), (Huescar (HU), Teruel (TE), Zaragoza (Z)); Castilla y León (CL) (Ávila, (AV), Burgos (BU), León (LE), Palencia (P), Salamanca (SA), Segovia (SG),

Soria (SO), Valladolid (VA), Zamora (ZA)); Castilla La Mancha (CM) (Albacete (AB), Ciudad Real (CR), Cuenca (CU), Guadalajara (GU), Toledo (TO)); Canaria (CN) (Gran Canaria (GC), Tenerife (TF)); Cataluña (CT) (Barcelona (B), Girona (GI), Lleida (L), Tarragona (T)); Comunidad Valenciana (VC) (Alicante (A), Castellón (CS), Valencia (V)); Extremadura (EX) (Badajoz (BA), Cáceres (CC)); Galicia (GA) (A Coruña (C), Lugo (LU), Ourense (OR), Pontevedra (PO)); and País Vasco (PV) (Vizcaya (BI), Guipúzcoa (SS), Álava (VI)). One can observe at Soria (Castilla–León) and Barcelona (Cataluña), the limit LOOCV error values (see also Figure 1 below, and Figures 11–12 in the Supplementary Material). The LOOCV error mean is **0.1029395349**.

Data and **Step 4** output visualization, in terms of monthly averaged COVID–19 incidence maps, and their bayesian functional regression estimates, based on the overall sample, are displayed in Figures 1–10 in Section 1 of the Supplementary Material.

Region	P1	P2	P3	P4	P5	P6	P7	P8	P9
AN	AL	CA	CO	GR	H	J	MA	SE	
	0.0321	0.0694	0.0836	0.1275	0.0217	0.0775	0.1475	0.2082	
AR	HU	TE	Z						
	0.0197	0.0201	0.1268						
CL	AV	BU	LE	P	SA	SG	SO	VA	ZA
	0.0342	0.0750	0.0972	0.0370	0.0894	0.0449	0.0178	0.1505	0.0313
CM	AB	CR	CU	GU	TO				
	0.0511	0.1494	0.0452	0.0648	0.1939				
CN	GC	TF							
	0.0738	0.0553							
CT	B	GI	L	T					
	0.9516	0.0843	0.0630	0.0715					
EX	BA	CC							
	0.0831	0.0746							
GA	C	LU	OR	PO					
	0.0863	0.0180	0.0596	0.0617					
PV	BI	SS	VI						
	0.1938	0.1002	0.0839						
VC	A	CS	V						
	0.1383	0.0330	0.2003						

Table 1: *LOOCV errors after running 993 iterations*

4.2 Estimation algorithm two

As commented in Section 4.1, the data preprocessing procedure applied in **Step 1** of the estimation algorithm 2 is almost the same to the one applied in algorithm 1, considering, in addition, data tapering, which improves computations of the spatial functional spectral estimators. **Step 2** is then implemented after detrending the data. Specifically, denoting by X the detrended data, the empirical long–run spatial covariance operator $\widehat{\mathcal{R}}_{(\mathbf{N})}^X = \sum_{\mathbf{z} \in [0, T-1]^d} \widehat{\mathcal{R}}_{\mathbf{z}}$ is computed for $d = 2$, from the empirical spatial covariance operators (see also Figure 13

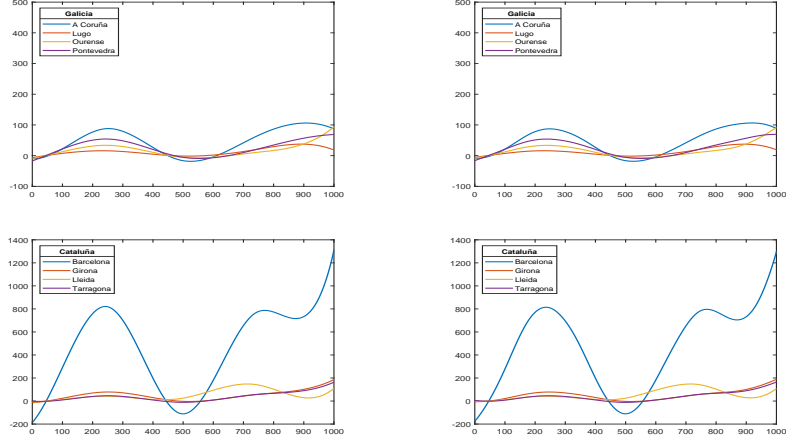


Figure 1: *Original data (left-hand-side), and Bayesian regression predictions (right-hand-side) at Galicia (top) and Cataluña (bottom)*

in the Supplementary Material):

$$\widehat{\mathcal{R}}_{\mathbf{z}} = \frac{1}{\prod_{i=1}^d T_i - z_i} \sum_{y_i \geq z_i, i=1, \dots, d} X_{\mathbf{y}} \otimes X_{\mathbf{y}-\mathbf{z}}, \quad \mathbf{z} \in [0, T-1]^d. \quad (29)$$

As output of **Step 3**, the singular value decomposition of $\widehat{\mathcal{R}}_{(\mathbf{N})}^X$ is obtained by calculating the empirical right $\{\psi_k^{(\mathbf{N})}\}_{k \geq 1}$, and left $\{\varphi_k^{(\mathbf{N})}\}_{k \geq 1}$ eigenvectors, and the corresponding singular values $\{\lambda_k(\widehat{\mathcal{R}}_{(\mathbf{N})}^X)\}_{k \geq 1}$ satisfying

$$\widehat{\mathcal{R}}_{(\mathbf{N})}^X \psi_k^{(\mathbf{N})} = \lambda_k(\widehat{\mathcal{R}}_{(\mathbf{N})}^X) \varphi_k^{(\mathbf{N})}, \quad k \geq 1.$$

For $k = 1, \dots, M$, after projection onto $\psi_k^{(\mathbf{N})}$, we compute **Step 4** from

$$\widetilde{X}_{\boldsymbol{\omega}}^{(\mathbf{N})}(\psi_k^{(\mathbf{N})}) = ((2\pi)^d \mathbf{N})^{-1/2} \sum_{\mathbf{z} \in [1, T]^d \cap \mathbb{Z}^d} X_{\mathbf{z}}(\psi_k^{(\mathbf{N})}) \exp(-i \langle \boldsymbol{\omega}, \mathbf{z} \rangle) \quad (30)$$

for $\boldsymbol{\omega} \in \{2\pi \mathbf{z}/T, \mathbf{z} \in [1, T-1]^d\}$, where the truncation parameter value $M = 5$ has been selected corresponding to a 99% of the empirical variability $\sum_{k=1}^M \lambda_k(\widehat{\mathcal{R}}_{(\mathbf{N})}^X)$. In **Step 5**, we obtain the corresponding projected periodogram operator

$$\mathcal{I}_{\boldsymbol{\omega}}^{(\mathbf{N})}(\psi_k^{(\mathbf{N})})(\psi_l^{(\mathbf{N})}) = \widetilde{X}_{\boldsymbol{\omega}}^{(\mathbf{N})}(\psi_k^{(\mathbf{N})}) \overline{\widetilde{X}_{\boldsymbol{\omega}}^{(\mathbf{N})}(\psi_l^{(\mathbf{N})})}, \quad k, l \in \{1, \dots, M\}, \quad (31)$$

for $\boldsymbol{\omega} \in \{2\pi \mathbf{z}/T, \mathbf{z} \in [1, T-1]^d\}$. In **Step 6**, the nonparametric estimator of the spectral density operator is then computed from equation (24), by considering a separable spatial version of the modified Bartlett–Hann window, corresponding to run *blackmanharris* at the first argument in the MatLab function

$window(\cdot, \cdot)$ (see left column in Figure 2, where two diagonal projections of the nonparametric spectral density operator estimator are displayed, and Figure 14 in the Supplementary Material). **Step 7** provides the calculation of equation (28) in the projected spatial functional spectral domain. **Step 8** applies $ifft2(\cdot, \cdot)$ MatLab function to the output in **Step 7** to obtain $\widehat{Y}_{S,N}$ (see Figure 3). See also right column in Figure 2. **Step 9** is finally computed by running nine times **Steps 1–8**. Specifically, for $n = 1, \dots, 9$, at the n th iteration, after removing the n th row and n th column, **Steps 1–8** are run from the remaining spatial curves defining the training sample. After evaluate the absolute errors obtained at each iteration, by comparing the output of **Steps 1–8** with the target curve sample, the mean over the nine iterations defines the curve absolute cross-validation errors over a 9×9 grid (see Figures 15, and Tables 1–4 of the Supplementary Material). Here, the average over the 1061 temporal nodes of the pointwise values of the absolute cross-validation errors are displayed in Table 2. See also Figure 16 in the Supplementary Material. Note that the mean of the pointwise values of the curve absolute cross-validation errors over the 1061 temporal nodes and 81 spatial nodes is **0.012789241**.

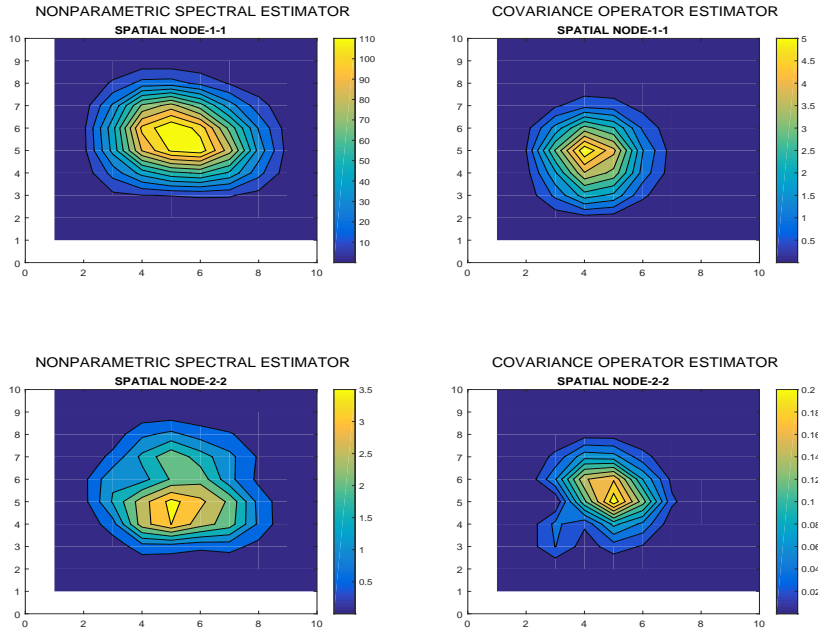


Figure 2: The projected nonparametric estimator of the spectral density operator $\widehat{f}_{\omega}^{(N)}(\psi_k)(\psi_l)$, for $k = l = 1$ (top-left-hand side), and for $k = l = 2$ (bottom-left-hand side). The corresponding projected spatial covariance operator estimates are displayed, for $k = l = 1$ (top-right-hand side), and for $k = l = 2$ (bottom-right-hand side)

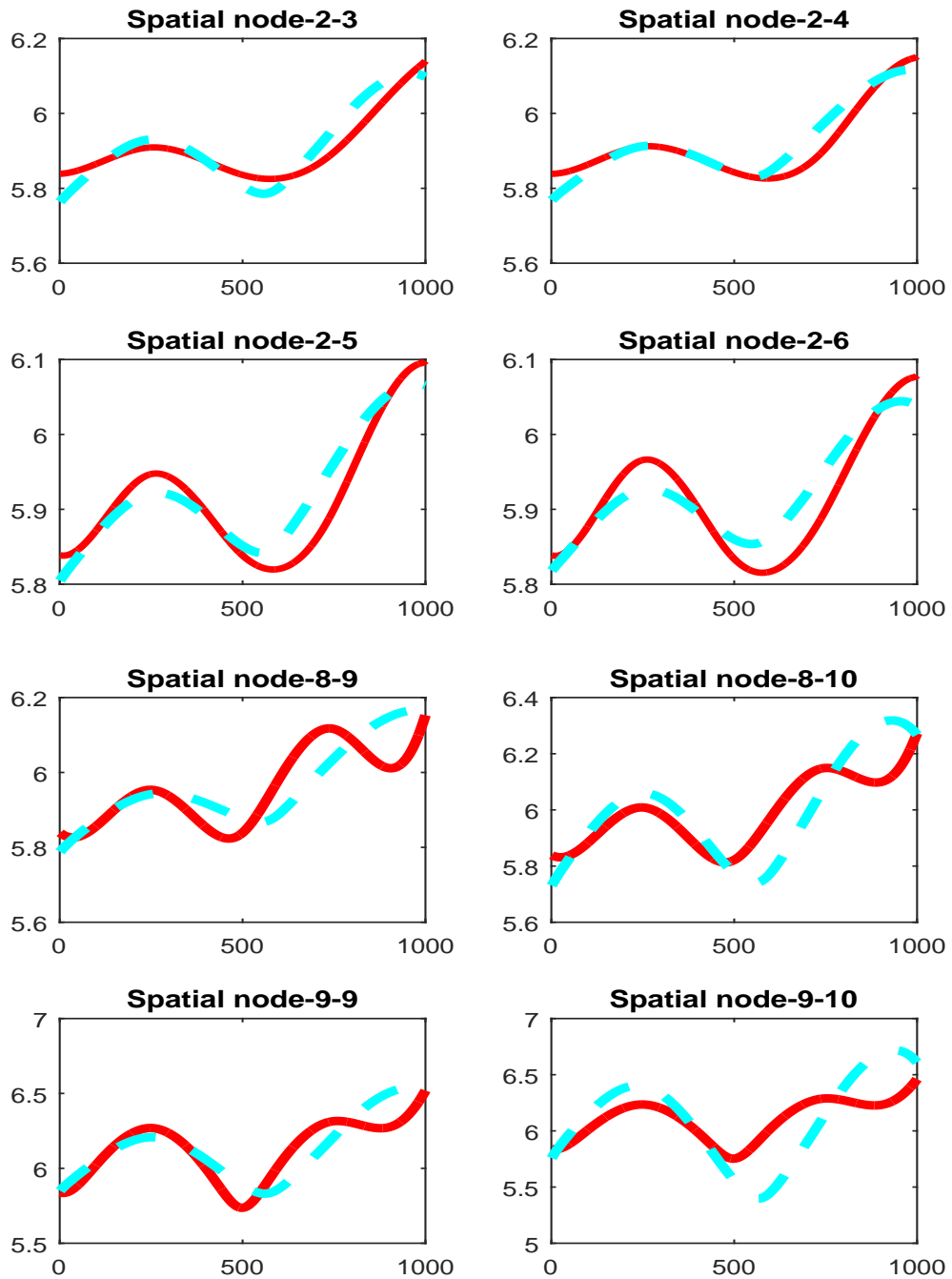


Figure 3: The original curve value (red line), and its spatial functional spectral estimate (dashed blue line) are displayed at the spatial nodes (2,3), (2,4), (2,5), (2,6), (8,9), (8,10), (9,9) and (9,10).

TIME	C1	C2	C3	C4	C5	C6	C7	C8	C9
R1	5.7030092e-04	6.8348935e-04	7.3573629e-04	1.2111422e-03	1.5253610e-03	1.1582524e-03	6.4996599e-04	4.4853841e-04	4.8335842e-04
R2	6.8117054e-04	1.0439449e-03	2.3038393e-03	4.3216034e-03	5.6747546e-03	4.0800204e-03	1.9086671e-03	9.3589234e-04	6.3663570e-04
R3	1.1343173e-03	4.9980942e-03	1.0964759e-02	2.1721765e-02	1.3553450e-02	1.2758592e-02	7.1904923e-03	2.7851634e-03	1.1143095e-03
R4	1.9814737e-03	7.4492915e-03	1.8550020e-02	5.9885317e-02	1.7065638e-01	4.3752536e-02	1.2645345e-02	5.5759098e-03	1.3117121e-03
R5	1.6909117e-03	9.1699655e-03	2.1533640e-02	3.8610072e-02	7.9602583e-02	1.4071528e-01	2.3334549e-02	7.4936816e-03	1.9115134e-03
R6	1.7947759e-03	8.3489455e-03	2.4934251e-02	3.4649351e-02	1.8313565e-02	2.7779579e-02	1.8405330e-02	6.5693512e-03	2.0597864e-03
R7	1.2888168e-03	5.1579564e-03	1.5046107e-02	2.1652733e-02	1.7133585e-02	8.0797335e-03	7.9961038e-03	3.1094061e-03	1.1663059e-03
R8	6.9762041e-04	1.7261479e-03	4.6013923e-03	9.2542787e-03	1.1597638e-02	7.8890004e-03	5.9333870e-03	2.0044843e-03	8.3627742e-04
R9	5.7529370e-04	6.4731393e-04	1.4868305e-03	3.0378125e-03	4.5606010e-03	4.1239116e-03	1.1999598e-03	6.9900174e-04	4.2810584e-04

Table 2: Average over the 1061 temporal nodes of the absolute cross-validation errors on a 9×9 grid

5 Final comments

This paper proposes two estimation methodologies in the context of functional regression. The first one is based on a bayesian approximation to the functional temporal correlation structure driving a surface functional time series analysis of spatiotemporal data. Here, our analysis is focused on computing the functional regression predictor of dynamical COVID-19 incidence maps at some Spanish Autonomous Communities. In this analysis, LOOCV absolute errors are computed to test the suitability of the prediction methodology proposed in an infinite-dimensional multivariate functional regression framework.

In a second place, we adopt a spatial curve time series framework to predict COVID-19 incidence from the estimation of the spatial curve correlation structure in the spectral domain. For dimension reduction in the time domain, projection onto the empirical long-run spatial covariance operator eigenvectors is achieved. It can be observed that the most significant spatial correlations through time are kept at the projections corresponding to the empirical eigenvectors associated with the largest singular values, explaining a 99% of the empirical variability. Indeed, the inverse spatial functional Fourier transform of the computed nonparametric estimator of the spectral density operator keeps the most significant correlation values at the diagonal projections. This projected correlation structure decays for cross projections, and goes to zero relatively fast, when we consider projections involving the empirical eigenvectors associated with the smallest empirical singular values.

To measure the predictive capability of the two functional regression approaches cross-validation is applied. In the surface regression framework, LOOCV is implemented by computing, according to equation (1), for $n = 1, \dots, 993$, the surface regression predictor $\hat{\mathbf{Y}}_{B,N,n}$ in (19) at time n , from the componentwise Bayesian estimate of the temporal surface correlation structure, based on the remaining 992 surfaces defining the training sample. This predictor is evaluated and compared with the target surface located at the temporal node n , eliminated in the definition of the surface training sample, for $n = 1, \dots, 993$. Note that 61 surfaces from the initial sample of 1061 surfaces are eliminated to remove edge effects. The remaining 7 surfaces at the initial times conform the random initial condition structure required to run equation (1) with $p = 7$.

A 9-fold cross validation technique is implemented to test the predictive

performance of estimation algorithm 2. The spatial geometric characteristics of our functional sample requires us to design a different cross-validation strategy. Specifically, the curves at the spatial nodes of the first row and column are needed to conform our random initial condition structure. The remaining spatial curves are split into a training and validation samples at each one of the iterations of the cross-validation procedure. Thus, we compute the empirical long-run spatial covariance operator and the non-parametric estimator of the spectral density operator from the training sample, as well as the corresponding curve regression predictor according to equation (28) (see also Section 3.1). Here, again, this predictor is compared with the target curves located at the n th row and n th column, for each one of the $n = 1, \dots, 9$ iterations.

We think that the worst performance observed in the implementation of the Bayesian surface regression is due to the more complex structure of the estimation methodology adopted, involving high-dimensional hyperparameters and parameter to be fitted. The spatial Markovian nature of the curve data analyzed allows us an easy and fast implementation of the spatial functional spectral approach. Specifically, dimension reduction by projection of the curve data onto the empirical eigenvectors of the long-run spatial covariance operator, and the faster computation speed obtained, replacing convolutions by products in the spatial functional spectral domain, favors the linear functional regression filter calculations under this approach.

Acknowledgements

This work has been supported in part by project MCIN/AEI/PGC2018-099549-B-I00 and CEX2020-001105-M MCIN/AEI/10.13039/501100011033.

References

- [1] Aneiros-Pérez, G., Cao, R. and Vilar-Fernández, J.M. (2011). Functional methods for time series prediction: a nonparametric approach. *J. Forecasting* 30:377–392.
- [2] Aneiros-Pérez, G. and Vieu, P. (2006). Semi-functional partial linear regression. *Stat. Probab. Letters*. 76:1102–1110.
- [3] Aneiros-Pérez G, and Vieu, P. (2008). Nonparametric time series prediction: A semi-functional partial linear modeling. *J. Multivariate Anal.* 99:834–857.
- [4] Aue, A., Norinho, D.D., and Hörmann, S. (2015). On the prediction of stationary functional time series. *Journal of the American Statistical Association*. 110:378–392.

- [5] Aue, A., Horváth, L., and Pellatt, D.F. (2017). Functional generalized autoregressive conditional heteroskedasticity. *Journal of Time Series Analysis*. 38:3–21.
- [6] Aue, A., and Klepsch, J. (2017). Estimating functional time series by moving average model fitting. *arXiv:1701.00770*.
- [7] Bosq, D. (2000). *Linear Processes in Function Spaces*. Springer-Verlag, New York.
- [8] Cai, T. and Hall, P. (2006). Prediction in functional linear regression. *The Annals of Statistics*. 34:2159–2179.
- [9] Canale, A. and Ruggiero, M. (2016). Bayesian nonparametric forecasting of monotonic functional time series. *Electron. J. Statist.* 10:3265–3286.
- [10] Cardot, H. (1998). Convergence du lissage spline de la prévision des processus autorégressifs fonctionnels. *C. R. Acad. Sci. Paris Sér. I Math.* 326:755–758.
- [11] Crambes, C., Kneip, A. and Sarda, P. (2009). Smoothing splines estimators for functional linear regression. *Annals of Statistics*. 37:35–72.
- [12] Cuevas, A., Febrero, M. and Fraiman, R. (2002). Linear functional regression: the case of fixed design and functional response. *The Canadian Journal of Statistics*. 30:285–300.
- [13] Cuevas, A. (2014). A partial overview of the theory of statistics with functional data. *Journal of Statistical Planning and Inference* 147:1–23.
- [14] Cugliari, J. (2013). Conditional autoregressive Hilbertian processes. journal "arXiv:1302.3488.
- [15] Damon, J. and Guillas, S. (2002). The inclusion of exogenous variables in functional autoregressive ozone forecasting. *Environmetrics* 13:759–774.
- [16] Damon, J. and Guillas, S. (2005). Estimation and simulation of autoregressive Hilbertian processes with exogenous variables. *Stat. Inference Stoch. Process.* 8:185–204.
- [17] Didericksen, D. and Kokoszka, P. (2012). Empirical properties of forecast with the functional autoregressive model. *Comput. Statist.* 27:285–298.
- [18] El Hajj, L. (2011). Limit theorems for $D[0, 1]$ -valued autoregressive processes. *C. R. Acad. Sci. Paris Sér. I Math.* 349:821–825.
- [19] Ezzahrioui, M. and Ould-Saïd, E. (2010). Some asymptotic results of a non-parametric conditional mode estimator for functional time-series data. *Statist. Neerlandica* 64:171–201.

- [20] Febrero-Bande, M., Galeano, P. and Gonzalez-Manteiga, W. (2015). Functional principal component regression and functional partial least-squares regression: an overview and a comparative study. *International Statistical Review* doi.org/10.1111/insr.12116.
- [21] Ferraty, F. and Goia, A. and Vieu, P. (2002). Functional nonparametric model for time series: a fractal approach for dimension reduction. *Test* 11:317–344.
- [22] Ferraty, F., Goia, A., Salinelli, E. and Vieu, P. (2013). Functional projection pursuit regression. *TEST*. 22:293–320.
- [23] Ferraty, F., Van Keilegom, I. and Vieu, P. (2012). Regression when both response and predictor are functions. *J. Multivariate Anal.* 109:10–28.
- [24] Ferraty, F. and Vieu, P. (2006). *Nonparametric Functional Data Analysis: Theory and Practice*. Springer, New York.
- [25] Ferraty, F. and Vieu, P. (2011). Kernel regression estimation for functional data. In: Ferraty F, Romain Y (eds) *The Oxford Handbook of Functional Data Analysis*. Oxford University Press, Oxford, pp. 72–129
- [26] Gao, Y., Shang H.L. and Yang, Y. (2019). High-dimensional functional time series forecasting: An application to age-specific mortality rates. *Journal of Multivariate Analysis*. 170:232-243.
- [27] Goia, A. and Vieu, P. (2015). A partitioned Single Functional Index Model. *Computational Statistics*. 30:673–692.
- [28] Goia, A. and Vieu, P. (2016). An introduction to recent advances in high/infinite dimensional statistics. *Journal of Multivariate Analysis*. 146:1–6,
- [29] Górecki, T., Hörmann, S., Horváth, L. and Kokoszka, P. (2018). Testing normality of functional time series. *Journal of time series analysis*. 39:471–487.
- [30] Guillas, S. (2001). Rates of convergence of autocorrelation estimates for autoregressive Hilbertian processes. *Statist. Probab. Lett.* 55:281–291.
- [31] Guillas, S. (2002). Doubly stochastic Hilbertian processes. *J. Appl. Probab.* 39:566–580.
- [32] Hörmann, S. and Kokoszka, P. (2010). Weakly dependent functional data. *The Annals of Statistics*. 38:1845–1884.
- [33] Hörmann, S. and Kokoszka, P. (2012). Functional Time Series in *Time Series Analysis: Methods and Applications* 30:157–186.

- [34] Hörmann, S., Horváth, L. and Reeder, R. (2013). A functional version of the ARCH model. *Econometric Theory*. 29:267–288.
- [35] Hörmann, S., Kokoszka, P. and Nisol, G. (2018). Testing for periodicity in functional time series. *Annals of statistics*. 46:2960–2984.
- [36] Horváth, L. and Kokoszka, P. (2012). *Inference for functional data with applications*. Springer, New York.
- [37] Horváth, L., Husková, M. and Rice, G., (2013). Test of independence for functional data. *Journal of Multivariate Anal.* 117:100–119.
- [38] Horváth, L., Husková, M. and Kokoszka, P. (2010). Testing the stability of the functional autoregressive process. *J. Multivariate Anal.* 101:352–367.
- [39] Horváth, L., Kokoszka, P. and Rice, G. (2014). Testing Stationarity of Functional Time Series. *Journal of Econometrics* 179:66–82.
- [40] Jadhav, S., Koul, H.L. and Lu, Q. (2017). Dependent generalized functional linear models. *Biometrika*, 104:987-994.
- [41] Kara-Terki, N. and Mourid, T. (2016). Local asymptotic normality of Hilbertian autoregressive processes. *C. R. Acad. Sci. Paris Sér. I* 354:634–638.
- [42] Kargin, V. and Onatski, A. (2008). Curve forecasting by functional autoregression. *J. Multivariate Anal.* 99:2508–2526.
- [43] Klepsch, J., Klüppelberg, C. and Wei T. (2017). Prediction of functional ARMA processes with an application to traffic data, *Econometrics and Statistics*. 1:128–149.
- [44] Kokoszka, P. and Reimherr, M. (2013a). Asymptotic normality of the principal components of functional time series. *Stochastic Process. Appl.* 123:1546–1562.
- [45] Kokoszka, P. and Reimherr, M. (2013b). Determining the order of the functional autoregressive model. *J. Time Ser. Anal.* 34:116–129.
- [46] Kowal, D.R., Matteson, D.S. and Ruppert, D. (2017). Functional autoregression for sparsely sample data. *J. Bus. Econom. Statist.* 37:97–109.
- [47] Labbas, A. and T. Mourid, T. (2002). Estimation et prévision d'un processus autorégressif Banach. *C. R. Acad. Sci. Paris Sér. I* 335:767–772.
- [48] Li, D., Robinson, P.M., and Shang, H.L. (2020). Long-range dependent curve time series. *Journal of the American Statistical Association*. 115:957–971.

- [49] Liu, X., Xiao, H. and Chen, R. (2016). Convolutional autoregressive models for functional time series. *J. Econometrics* 194:263–282.
- [50] Laukaitis, A. (2008). Functional data analysis for cash flow and transactions intensity continuous-time prediction using Hilbert-valued autoregressive processes. *European J. Oper. Res.* 185:1607–1614.
- [51] Marion, J. M. and Pumo, B. (2004). Comparison of ARH(1) and ARHD(1) models on physiological data. *Ann. I.S.U.P.* 48:29–38.
- [52] Marx, B.D., and Eilers, P.H.C. (1999). Generalized linear regression on sampled signals and curves: A P-spline approach. *Technometrics*, 41:1–13.
- [53] Mas, A. (1999). Normalité asymptotique de l'estimateur empirique de l'opérateur d'autocorrélation d'un processus ARH(1). *C. R. Acad. Sci. Paris Sér. I Math.* 329:899–902.
- [54] Mas, A. (2000). Estimation d'opérateurs de corrélation de processus fonctionnels: lois limites, tests, déviations modérées. Université de Paris 6. Paris.
- [55] Mas, A. (2002). Weak convergence for the covariance operators of a Hilbertian linear process. *Stochastic Process. Appl.* 99:117–135.
- [56] Mas, A. (2004). Consistance du prédicteur dans le modèle ARH(1): le cas compact. *Ann. I.S.U.P.* 48:39–48.
- [57] Mas, A. (2007). Weak-convergence in the functional autoregressive model. *J. Multivariate Anal.* 98:1231–1261.
- [58] Mas, A. and Menneteau, L. (2003). Large and moderate deviations for infinite dimensional autoregressive processes. *J. Multivariate Anal.* 87:241–260.
- [59] Mas, A. and Pumo, B. (2007). The ARHD model. *J. Statist. Plann. Inference* 137:538–553.
- [60] Morris, J.S. (2015). Functional regression. *Annual Review of Statistics and Its Application* 2:321-359.
- [61] Panaretos, V.M. and Tavakoli, S. (2013a). Fourier analysis of stationary time series in function space. *The Annals of Statistics*. 41:568–603.
- [62] Panaretos, V. M. and Tavakoli, S. (2013b). Cramér—Karhunen—Loève representation and harmonic principal component analysis of functional time series. *Stochastic Process and their Applications*. 123:2779–2807.
- [63] Petris, G.A. (2013). Bayesian framework for functional time series analysis. arXiv:1311.0098v2.

- [64] Pham T. and Panaretos V. (2018). Methodology and convergence rates for functional time series regression. *Statistica Sinica*. 28:2521—2539. (Special Issue in Memory of Peter Hall).
- [65] Ramsay, J.O. and Silverman, B.W. (2005). *Functional data analysis, Second Ed.* Springer Series in Statistics. Springer, New York.
- [66] Rubín, T. and Panaretos, V.M. (2020a). Functional lagged regression with sparse noisy observations. *Journal of Time Series Analysis*. 41:858–882.
- [67] Rubín, T. and Panaretos, V.M. (2020b). Spectral simulation of functional time series. *arXiv preprint arXiv:2007.08458*.
- [68] Ruiz-Medina, M.D. (2016). Functional analysis of variance for Hilbert-valued multivariate fixed effect models. *Statistics*. 50:689–715.
- [69] Ruiz-Medina, M.D. (2021). Spectral analysis of long range dependence functional time series. *arXiv:1912.07086*.
- [70] Ruiz-Medina, M.D., Miranda, D. and Espejo, R.M. (2019). Dynamical multiple regression in function spaces, under kernel regressors, with ARH(1) errors. *Test* 28:943-968.
- [71] Tavakoli, S. (2014). Fourier Analysis of Functional Time Series, With Applications to DNA Dynamics, Ph.D. dissertation, EPFL. Available at <http://dx.doi.org/10.5075/epfl-thesis-6320>.
- [72] Tavakoli, S. and Panaretos, V.M. (2016). Detecting and localizing differences in functional time series dynamics: a case study in molecular biophysics. *Journal of the American Statistical Association*. 111:1020–1035
- [73] Torres--Signes, A, Frías, M.P. and Ruiz-Medina, M.D. (2021). COVID–19 mortality analysis from soft-data multivariate curve regression and machine learning. *Stochastic Environmental Research and Risk Assessment*. doi.org/10.1007/s00477-021-02021-0.
- [74] Wang, J.L., Chiou, J.M., and Müller, H.G. (2016). Functional data analysis. *Annual Review of Statistics and Its Application*, 3:257-295.